

# Raman solitons in transient SRS\*

M. Boiti<sup>+</sup>, J-G. Caputo, J. Leon, F. Pempinelli<sup>+</sup>  
*Physique Mathématique et Théorique, CNRS-UMR5825,*  
 Université Montpellier 2, 34095 MONTPELLIER (France)  
 (+) *and Dipartimento di Fisica dell' Università, Lecce (Italy)*

## Abstract

We report the observation of Raman solitons on numerical simulations of transient stimulated Raman scattering (TSRS) with small group velocity dispersion. The theory proceeds with the inverse scattering transform (IST) for initial-boundary value problems and it is shown that the explicit theoretical solution obtained by IST for a semi-infinite medium fits strikingly well the numerical solution for a finite medium. We understand this from the rapid decrease of the medium dynamical variable (the potential of the scattering theory). The spectral transform reflection coefficient can be computed directly from the values of the input and output fields and this allows to see the generation of the Raman solitons from the numerical solution. We confirm the presence of these nonlinear modes in the medium dynamical variable by the use of a discrete spectral analysis.

## 1 Introduction

Stimulated Raman scattering (SRS) is a 3-wave interaction process with extremely wide application in physics, especially in nonlinear optics [1][2]. This essentially nonlinear phenomenon couples two electromagnetic waves (pump and Stokes waves) to a two-level medium and is described by a simple system of partial differential equations [3].

Such a system applies to different physical situations, depending on a phenomenological damping factor chosen to match the observed Raman linewidth. For instance, the steady state regime occurs when one neglects dynamical effects on the medium. Then the system becomes explicitly solvable in terms of the intensities and the result fits well the situation of strong damping and long pulses, such as in fiber guides [4]. When instead dynamical effects and damping are of same order, very interesting phase effects have been discovered in [5]. These have been interpreted as the manifestation of solitons which, in the spectral

---

\*to appear in Inverse Problems

transform scheme, would be related to discrete eigenvalues. Instead they are related to the continuous spectrum (they are not solitons) and named *Raman spikes* [6]. Therefore the question of the observation of the Raman soliton is open since the original work [3] in 1975.

When the damping term is much smaller than the dynamical response of the medium, and can be neglected the regime is called hyper-transient and applies to short duration pulses. Here the system possesses a Lax pair [3, 7, 8] and can be treated by means of the inverse scattering transform (IST) generalized to boundary-value problems [9, 10]. The observation of the Raman soliton is an interesting open problem, especially since the boundary-value problem for TSRS has been completely solved on the finite interval in [11] with the essential result that, as expected from the works [12, 13, 14], the field  $q(x, t)$  universally evolves toward the self-similar solution.

The commonly used TSRS model is obtained as a 3-wave interaction process where the group velocities of the 3 fields involved are considered equal. As shown in [15], this assumption is an asymptotic limit and consequently the group velocity dispersion (GVD) has to be taken into account (through the spectral extension of the input laser fields), leading to a modified SRS system (eq. (2.2) below). The main consequence of this fact is that Raman solitons (discrete eigenvalues in the nonlinear Fourier spectrum) are effectively generated by SRS in the medium [15].

The aim of this paper is to show that Raman solitons are indeed created in a finite length medium and that their generation is accompanied with poles in the nonlinear Fourier spectrum (spectral transform). We follow the model derived and solved in [15] and establish the following results.

1 - Based on the assumption of a semi-infinite medium, IST gives an explicit solution<sup>1</sup> which will be shown to be an excellent approximation of the finite medium case. We explain this from the fast decay of the *potential*  $q(x, t)$  for large  $x$ . Such is not the case in the zero-GVD case for which  $q(x, t)$  decreases as  $x^{-3/4}$  typical of the self-similar solution [12, 11].

2 - The reflection coefficient  $\rho$  of the spectral transform (or nonlinear Fourier spectrum) is expressed in terms of the input and output field envelopes, allowing us to check the appearance of Raman solitons (the real valued single poles of  $\rho$ ) on the numerical solutions. This also provides a means to observe the generation of Raman solitons in experimental data.

3 - A recursion formula for computing the spectral transform of a finite set of data has been recently proposed [16]. We have implemented this *discrete spectral transform* and confirmed the creation of these Raman solitons in a simulation on a finite length. A remarkable feature here is that the numerical spectral transform can be quite easily implemented, its computation is faster, and it provides more information than a conventional Fourier transform.

---

<sup>1</sup>The solution is not explicit for the finite length case: both results of [15] and of [11] give the answer by solving a system of Cauchy-Green integral equations.

After presenting the model in section 2, we report the numerical observation of the Raman solitons in section 3. Section 4 explains this by an analysis of the medium dynamical variable.

## 2 The model

We present here the extension of the SRS model of [3] to the case where the dispersion of the group velocity is not neglected. We consider the classical model as in [2], well adapted to molecular Raman scattering, and for which the medium is schematically represented by a collection  $X$  of harmonic oscillators coupled to the electric field  $\vec{E}$  through the polarizability of the medium.

### 2.1 Basic equations

When the polarizability depends on the frequency of the applied field, the group velocity of the electromagnetic waves becomes frequency dependent. While a very small group velocity dispersion (GVD) has no consequence on the evolution of the amplitude, it has nontrivial effects on the phase dynamics. In this context, it has been proved in [15], using *multiscale analysis*, that for the electric field

$$E(x, t') = e^{i(k_1 x - \omega_1 t')} \int dk a(k, x, t) e^{-ikx} + e^{i(k_2 x - \omega_2 t')} \sqrt{\frac{\omega_2}{\omega_1}} \int dk b(k, x, t) e^{ikx} + c.c. \quad (2.1)$$

and medium dynamical variable  $q(x, t) e^{i(Kx - \Omega t')} + c.c.$  where  $\omega_1 - \omega_2 = \Omega$  and  $k_1 - k_2 = K$ , the resulting model of transient SRS can be written in the *retarded time*  $t = t' - x/v$

$$\begin{aligned} \partial_x a &= q b e^{2ikx}, \quad \partial_x b = -\bar{q} a e^{-2ikx}, \\ \partial_t q &= -g \int dk a \bar{b} e^{-2ikx}, \end{aligned} \quad (2.2)$$

where the overbar stands everywhere for the complex conjugate. Note the conservation ( $x$ -independence) of the flux density  $|a|^2 + |b|^2$ .

The above model differs from the usual SRS system, corresponding to the zero GVD case

$$\partial_x a = q_0 b, \quad \partial_x b = -\bar{q}_0 a, \quad \partial_t q_0 = -g a \bar{b}, \quad (2.3)$$

by the presence of the integral over all possible realizations of the phase mismatch  $k$ .

## 2.2 Boundary value problem

The question of interest is the time evolution of a couple  $(a, b)$  of pump and Stokes pulses of time duration  $T$  sent into a medium of length  $\ell$ . Hence the domain of integration is

$$x \in [0, \ell] , \quad t \in [0, T] . \quad (2.4)$$

and it is necessary to prescribe the values of the fields on the two boundaries  $t = 0$  and  $x = 0$ . The medium is initially ( $t = 0$ ) at rest (all molecules in the fundamental state), hence the initial datum for the field  $q$  is

$$q(x, 0) = 0 , \quad (2.5)$$

independently of the reference frame <sup>2</sup>.

The input ( $x = 0$ ) light pulses are arbitrary functions of time  $t$  with a given spectral distribution around  $k = 0$ , namely

$$a(k, 0, t) = A(k, t) , \quad b(k, 0, t) = B(k, t) . \quad (2.6)$$

We shall be working here with the representative example treated in [15] which consists in assuming a common spectral lineshape for  $A$  and  $B$  as a normalized Lorentzian lineshape for the intensities. More precisely we set

$$|A(k, t)|^2 = |A_0(t)|^2 \frac{1}{\pi} \frac{\kappa}{k^2 + \kappa^2} , \quad |B(k, t)|^2 = |B_0(t)|^2 \frac{1}{\pi} \frac{\kappa}{k^2 + \kappa^2} , \quad (2.7)$$

where the input pulse profiles  $A_0(t)$  and  $B_0(t)$  are arbitrary.

It is useful also to understand the scale invariance of the SRS system, including its boundary values. By a simple change of variables it can be easily shown that the system (2.2) (characterized by the parameters  $g$  and  $\ell$ ) *together with* the input boundary values (2.6) (2.7) (characterized by the parameter  $\kappa$ ) bears the scale invariance

$$\ell \rightarrow \alpha \ell , \quad g \rightarrow g/\alpha , \quad \kappa \rightarrow \kappa/\alpha . \quad (2.8)$$

This invariance has been checked on numerical simulations as one way to test the code accuracy, and it works so well that we have obtained indiscernible pictures.

## 3 Laser fields

We describe hereafter the IST solution of the boundary-value problem (2.6) for the system (2.2) using the results of [15], and compare it with the direct numerical solution in the finite length case.

---

<sup>2</sup>Note that a *prepared* medium would correspond to a state  $q$  given at *physical time* zero, that is on the characteristic  $t = -x/v$ .

### 3.1 Sketch of the direct problem

The direct problem consists in defining the spectral transform from the data of the *potential*  $q(x, t)$  and the boundary values  $A(k, t)$  and  $B(k, t)$  (as time  $t$  appears everywhere as an external parameter, we shall forget it here). This is done by defining the following Jost solutions (for  $k \in \mathbb{R}$ )

$$\begin{aligned}\varphi(k, x) &= 1 - \int_0^x d\xi \, q(\xi) \phi(k, \xi) , \\ \phi(k, x) &= \int_0^x d\xi \, \bar{q}(\xi) \varphi(k, \xi) e^{2ik(x-\xi)} ,\end{aligned}\tag{3.1}$$

which are both entire functions of  $k$  vanishing as  $k \rightarrow \infty$  in the upper half-plane.

These two functions then allow to define the *reflection coefficient*  $\rho(k)$  and the *transmission coefficient*  $\tau(k)$  by taking the limit  $x \rightarrow \infty$  of  $\varphi$  and  $\bar{\phi}e^{2ikx}$  for  $k \in \mathbb{R}$ , namely

$$\frac{1}{\tau} = 1 - \int_0^\infty d\xi \, q(\xi) \phi(k, \xi) , \quad \frac{\rho}{\tau} = - \int_0^\infty d\xi \, q(\xi) \bar{\varphi}(k, \xi) e^{2ik\xi} .\tag{3.2}$$

The coefficient  $1/\tau$  is clearly an entire function of  $k$  and one can show [15] that the reflection coefficient  $\rho(k)$  is meromorphic in the upper half-plane with a finite number of single poles related to the solitonic part of the solution  $q$ . We have also the following *unitarity* relation for  $k \in \mathbb{R}$

$$|\rho|^2 = 1 + |\tau|^2 .\tag{3.3}$$

It is easy to prove finally that the vectors  $(\varphi, -\phi e^{-2ikx})$  and  $(\bar{\phi}e^{2ikx}, \bar{\varphi})$  solve the same differential equation as the vector  $(a, b)$  in (2.2). Then by comparing their values in  $x = 0$  we readily obtain from (2.6)

$$a = A\varphi + B\bar{\phi}e^{2ikx} , \quad b = B\bar{\varphi} - A\phi e^{-2ikx} .\tag{3.4}$$

### 3.2 Output pump pulse

From (3.2), (3.3) and (3.4), the output  $|a(k, \ell, t)|^2$  is explicitly given for  $\ell \rightarrow \infty$  by the expression

$$|a(k, \infty, t)|^2 = \frac{1}{1 + |\rho|^2} |A - \rho B|^2 ,\tag{3.5}$$

where  $A$  and  $B$  are the input data defined in (2.6).

---

<sup>3</sup>The relation with notations of [15] is:  $\varphi(k) = \varphi_{11}^+(k) = \overline{\varphi_{22}^-}(\bar{k})$ ,  $\phi(k) = -\varphi_{21}^+(k) = \overline{\varphi_{12}^-}(\bar{k})$ .

The main result of [15] is that the function  $\rho(k, t)$  is obtained by solving the following Riccati time evolution

$$\rho_t = -\rho^2 \mathcal{C}_k^+[m^*] - 2\rho \mathcal{C}_k^+[\phi] - \mathcal{C}_k^+[m], \quad \rho(k, 0) = 0, \quad (3.6)$$

where the functions  $m(k, t)$  and  $\phi(k, t)$  are given from the input data by

$$m = \frac{i\pi}{2}gAB^*, \quad \phi = \frac{i\pi}{4}g(|A|^2 - |B|^2), \quad (3.7)$$

and where  $\mathcal{C}_k^+$  denote the following Cauchy integral

$$\mathcal{C}_k^+[f] = \frac{1}{\pi} \int_{-\infty}^{+\infty} \frac{d\zeta}{\zeta - (k + i0)} f(\zeta). \quad (3.8)$$

Consequently, for given inputs  $A(k, t)$  and  $B(k, t)$ , the expression (3.5) gives the explicit asymptotic output pump intensity from the solution of the evolution (3.6). It is worth remarking that, at any given time,  $\rho$  possesses possibly a finite number of simple poles whose time evolution is given by the nonlinearity of the Riccati equation.

For practical purpose, we choose in (2.6) the Stokes wave input seed as a portion  $e^{-\gamma}$  of the pump wave, namely

$$B_0(t) = A_0(t) e^{-\gamma}. \quad (3.9)$$

In that case the evolution (3.6) can be explicitly solved [15]

$$\rho(k, t) = \frac{\sinh \delta(k, t)}{\cosh(\delta(k, t) - \gamma)}, \quad (3.10)$$

$$\delta(k, t) = \frac{iT(t)}{k + i\kappa}, \quad T(t) = \frac{1}{4}g(1 + e^{-2\gamma}) \int_0^t d\tau |A_0(\tau)|^2. \quad (3.11)$$

### 3.3 Numerical solution of finite length TSRS

Our purpose is to understand how the above IST-solution can be used to model the solution of the SRS system (2.2) on a finite length. This can be done first in a qualitative way by writing the solution of (2.2) with boundary values (2.6) as the equivalent integral form

$$\begin{pmatrix} a(k, x, t) \\ b(k, x, t) \end{pmatrix} = \begin{pmatrix} A(k, t) \\ B(k, t) \end{pmatrix} + \int_0^x d\xi \begin{pmatrix} q(\xi, t)b(k, \xi, t)e^{2ik\xi} \\ -\bar{q}(\xi, t)a(k, \xi, t)e^{-2ik\xi} \end{pmatrix}. \quad (3.12)$$

The output  $a(k, \ell, t)$  will not differ much from its asymptotic value  $a(k, \infty, t)$  if  $q(x, t)$  is sufficiently small for  $x > \ell$ . Consequently the behavior of  $q(x, t)$  at large  $x$ , is essential for the adequation of the formula (3.5) to real situations. We will see in the next section that it is also crucial for the applicability of

the spectral method. We now proceed to show that the numerical solution of the TSRS system (2.2) on a finite interval is in excellent agreement with the theoretical expression for the output (3.5).

We discretized (2.2) in both  $x$  and  $t$  using an order 2 Runge-Kutta method and advance via the following algorithm:

- 1 - given  $a(k, x, t)$  and  $b(k, x, t)$  for all real  $k$ , compute  $q(x, t)$  by integrating the time-evolution of  $q$  at  $x$  for the initial datum  $q(x, t = 0) = 0$ , where the integral is calculated using the trapezoidal rule,
- 2 - advance to  $a(k, x + dx, t)$  and  $b(k, x + dx, t)$ , for all  $k$ , by integrating the differential equation for  $a$  and  $b$ ,
- 3 - go to step 1 with  $x = x + dx$ .

The scheme is started at step 1 for  $x = 0$ .

The quality of the computation is monitored by evaluating the relative error in the total flux  $|a(k, x, t)|^2 + |b(k, x, t)|^2$  which is conserved by (2.2). In all the runs that are presented it remained smaller than  $10^{-5}$ .

We chose as parameters

$$\ell = 80, \quad g = 0.5, \quad \gamma = 5, \quad \kappa = 0.2, \quad (3.13)$$

and the input pump pulse envelope is the Gaussian

$$A_0(t) = \exp \left[ - \left( \frac{t - 50}{30} \right)^2 \right]. \quad (3.14)$$

For this choice we found that  $dt \leq T/1000$  and  $dx \leq \kappa/2$  gave stable results. Another point is that because of the Lorentzian line width we had to take a  $k$  interval of width  $\approx 80\kappa$  in order to ensure that the integrals were normalized. To describe the strong oscillations present for the zero GVD system (2.3) we had to chose  $dt \leq T/2000$  and  $dx \leq \ell/10000$ .

A typical run with number of grid points in  $x, t$  and  $k$  ( $n_x = n_t = 1000; n_k = 500$ ) takes about 2 hours CPU monoprocessor on a RS10000. We used the parallelism of the problem, i.e. the fact that the marching in  $x$  (resp.  $t$ ) can be made in parallel for the loops in  $t$  and  $k$  (resp.  $x$ ) and implemented the code on a Silicon Graphics SGI 10000 using the OpenMP software. This enabled a gain of a factor 8 or 10 in computing time depending on the number of processors used.

Figure 1 show the pump intensity input  $|a(k, 0, t)|^2$  and output  $|a(k, \ell, t)|^2$  computed from the IST expression (3.5) together with the numerical solution of the system (2.2) for a length  $\ell = 80$  and four different values of the parameter  $k$ , in excellent agreement (a tiny discrepancy is only seen in the last picture).

It is worth remarking that one cannot pursue a given numerical experiment to a longer length arbitrarily. We have stopped for instance the above calculation at length  $\ell = 80$  where the potential  $|q(x, t)| < 10^{-5}$ . Continuing the run to longer lengths would yield an increase of the potential which would then start to

oscillate. This is probably due to the system itself which amplifies the numerical errors in a drastic way at long lengths (note that from the scale invariance (2.8) longer length means larger Raman amplification).

### 3.4 Raman solitons

The function  $\rho$  of (3.10) has an essential singularity in  $k = -i\kappa$  and a set of single poles  $k_n$  evolving in time, given by

$$k_n(t) = -i\kappa + \frac{T(t)}{(n + \frac{1}{2})\pi - i\gamma} , \quad (3.15)$$

for  $n \in \mathbb{N}$ . At time zero no pole is present and, as  $t$  evolves, poles move upward from  $-i\kappa$  and eventually reach the real axis at the times  $t_n$  defined by  $\text{Im}(k_n(t_n)) = 0$ , i.e. by the implicit expression

$$T(t_n) = \frac{\kappa}{\gamma} [\gamma^2 + [(n + \frac{1}{2})\pi]^2] . \quad (3.16)$$

Note that  $t_n = t_{-n-1}$ , hence the poles cross the real axis by pair. The corresponding positions on the real axis are then given by

$$k_n(t_n) = -k_{-n-1}(t_n) = \zeta_n , \quad \zeta_n = \frac{\kappa}{\gamma} (n + \frac{1}{2})\pi . \quad (3.17)$$

We plot in Figure 2 the imaginary part of the poles  $k_n(t)$  as a function of time for the parameter values (3.13) and  $n = 0, 1, 2$  and 3. We observe that the first three poles cross the real axis at the positions  $\zeta_0 = 6.310^{-2}$ ,  $\zeta_1 = 0.19$ ,  $\zeta_2 = 0.31$  and times  $t_0 = 39.2$ ,  $t_1 = 46.3$  and  $t_2 = 59.6$ . The pole  $k_3$  starts to evolve with  $t$  but cannot cross the real axis because of the finite duration of the pump pulse.

As soon as these poles move to the upper half-plane, they generate a soliton component in the "potential"  $q(x, t)$ . We will prove in the next section that this potential (the medium dynamical variable) is a continuous function of  $t$  when a pole crosses the real axis.

### 3.5 The spectral transform from the output laser pulses

The expressions (3.4) can be inverted to get the following expressions of the Jost solutions in terms of the (physical) fields  $a(k, x, t)$  and  $b(k, x, t)$  and of the input pulses  $A(k, t)$  and  $B(k, t)$

$$\varphi = \frac{a\bar{A} + \bar{b}B}{|A|^2 + |B|^2} , \quad \bar{\phi}e^{2ikx} = \frac{a\bar{B} - \bar{b}A}{|A|^2 + |B|^2} . \quad (3.18)$$

Then the definitions (3.2) lead to the following formula

$$\rho(k, t) = \frac{\bar{b}A - a\bar{B}}{a\bar{A} + \bar{b}B} \Big|_{x \rightarrow \infty} \quad (3.19)$$



which gives the spectral transform  $\rho(k, t)$  in terms of the output pump and Stokes fields. This function for  $k$  real must become singular at the two points  $\pm\zeta_n$  each time a soliton  $k_n$  is created and it is used now to prove the generation of Raman solitons in numerical experiments.

For the input pulses given in (2.7) and the particular choice (3.9), we readily obtain from the above

$$\rho = \frac{\bar{b} - ae^{-\gamma}}{a + \bar{b}e^{-\gamma}} \Big|_{x \rightarrow \infty}. \quad (3.20)$$

We use this expression to estimate  $\rho_\ell$  from the numerical solution  $(a, b)$  at  $x = \ell < +\infty$  and compare it to the  $\rho$  obtained from the IST (3.10) for the parameters (3.13). Notice that  $|\rho(-k)| = |\rho(k)|$  so that we will only present positive values of  $k$ .

Figure 3 shows the function  $|\rho|$  of (3.10) in full line and the numerical result obtained from (3.20) in  $x = \ell$  the in dashed line, for the 3 values  $k = \zeta_0, \zeta_1, \zeta_2$  and  $\zeta_3$ . Both expressions are very close and as expected  $\rho(\zeta_n)$  is singular for  $t = t_n$  for  $n \leq 2$ , while it is regular for  $n = 3$ . In the first picture of figure 3, the dashed line actually represents the value at  $k = 0$  instead of  $k = \zeta_0$ . This is the only noticeable discrepancy between analytic asymptotic formula and numerical/experimental expression, resulting from the finiteness in  $x$  of the data  $q(x)$  (the wave length  $\lambda_0 \equiv 2\pi/\zeta_0 \approx 104 > \ell$ ).

## 4 Medium

In the previous section we have seen that the finite length solution is in good agreement with the asymptotic behavior (3.5) given by the IST on the semi-infinite line. We now proceed to justify this fact by analyzing the behavior of the medium dynamical variable  $q(x, t)$ .

### 4.1 Sketch of the inverse problem

IST furnishes the solution  $q(x, t)$ , called *medium dynamical variable*, by the expression [15]

$$q(x, t) = 2i\psi^{(1)}(x, t) \quad (4.1)$$

where  $\psi^{(1)}$  is the coefficient of  $1/k$  in the Laurent expansion of the function  $\psi(k, x, t)$  solution of the following Cauchy-Green coupled system

$$\begin{aligned} \varphi(k) &= 1 + \frac{1}{2i\pi} \int_{-\infty}^{+\infty} d\lambda \frac{\bar{\rho}(\lambda)\psi(\lambda)}{\lambda - k - i0} e^{2i\lambda x} - \sum_1^N \frac{\bar{\rho}(\bar{k}_n)\psi(\bar{k}_n)}{k - k_n} e^{2i\bar{k}_n x} \\ \psi(k) &= \frac{1}{2i\pi} \int_{-\infty}^{+\infty} d\lambda \frac{\rho(\lambda)\varphi(\lambda)}{\lambda - k + i0} e^{-2i\lambda x} + \sum_{n=1}^N \frac{\rho_n\varphi(k_n)}{k - k_n} e^{-2ik_n x}. \end{aligned} \quad (4.2)$$

Here  $\rho_n(t)$  are the  $N$  residues of  $\rho(k, t)$  at the poles  $k_n(t)$  that are in the upper half  $k$ -plane (if any). Note that the solution  $\varphi$  corresponds to the solution of (3.1) and that  $\psi(k) = \overline{\varphi(\bar{k})}$ .

Apparently the generation of a soliton is followed by the adjunction of a term in the equation for  $\psi$ , and consequently also in the expression of  $q$ , leading to a possible discontinuity for  $q$ . We will now proceed to show that this is not the case. This situation is particular to the spectral problem on the semi-line where the continuous spectrum (value of  $\rho(k)$  on the real axis) is not separable from the discrete spectrum (poles of  $\rho$  in the upper half complex plane). This is due to the motion of the poles of  $\rho$  that can cross the real axis. On the contrary, in the full line case, solitons (discrete spectrum) can exist without radiation (continuous spectrum).

## 4.2 Continuity

From now on when the spectral parameter  $k$  is generically complex we shall be using boldface letter  $\mathbf{k}$ . From what precedes, at  $t = t_0$  a pole crosses the real axis at  $k = k_0$  from the lower half plane. We consider here the limits  $t \rightarrow t_0 \pm 0$  and we write for  $k \in \mathbb{R}$

$$\rho_{\pm}(k) = \rho(k, t_0 \pm 0) = \frac{R_0(k)}{k - k_0 \mp i0} \quad (4.3)$$

where  $R_0(\mathbf{k})$  is analytic in a neighborhood of  $k_0$ . Note that

$$\rho_+(k) = \rho_-(k) + 2\pi i \rho_0 \delta(k - k_0) \quad (4.4)$$

where  $\rho_0 = R_0(k_0)$  is the residue of  $\rho$  at the pole  $k = k_0$ .

Assuming for simplicity no other pole, we have from (4.2) at  $t = t_0 - 0$

$$\psi(k, x, t_0 - 0) = \frac{1}{2i\pi} \int_{-\infty}^{+\infty} d\lambda \frac{\rho_-(\lambda) \varphi(\lambda, x, t_0 - 0)}{\lambda - k + i0} e^{-2i\lambda x} \quad (4.5)$$

which is well defined at  $k = k_0$  since the distribution  $(\lambda - k_0 + i0)^{-2}$  is meaningful.

On the contrary at  $t = t_0 + 0$ , expression (4.5) diverges due to the distribution  $(\lambda - k_0 + i0)^{-1}(\lambda - k_0 - i0)^{-1}$ . Since now there is a pole in the upper half complex plane, we should take the limit  $\text{Im}(\mathbf{k}) \rightarrow 0$  in the complete expression in (4.2). i.e.

$$\begin{aligned} \psi(\mathbf{k}, x, t_0 + 0) &= \frac{1}{2i\pi} \int_{-\infty}^{+\infty} d\lambda \frac{\rho_+(\lambda) \varphi(\lambda, x, t_0 + 0)}{\lambda - \mathbf{k}} e^{-2i\lambda x} \\ &\quad + \frac{\rho_0 \varphi(k_0, x, t_0 + 0)}{\mathbf{k} - k_0} e^{2ik_0 x}, \end{aligned} \quad (4.6)$$

for  $\text{Im}(\mathbf{k}) < 0$ . We obtain

$$\psi(k, t_0 - 0) = \psi(k, t_0 + 0). \quad (4.7)$$

and consequently from (4.1)

$$q(t_0 - 0) = q(t_0 + 0). \quad (4.8)$$

### 4.3 Asymptotic behavior

We consider here for simplicity the case when solitons are not yet present. Then from (4.1) and (4.2),  $q$  can be reconstructed in terms of the reflection coefficient  $\rho$  and the Jost solution  $\varphi$  by means of

$$q(x) = -\frac{1}{\pi} \int_{-\infty}^{+\infty} dk \, \rho(k) \varphi(k, x) e^{-2ikx}. \quad (4.9)$$

This formula yields directly an information on the behavior of  $q$  at large  $x$ .

In fact, if  $\rho(k)\varphi(k, x), \dots, \partial_k^{(n-1)}\{\rho(k)\varphi(k, x)\}$  are continuous and tend to 0 for  $k \rightarrow \infty$ , and if  $\partial_k^{(n)}\{\rho(k)\varphi(k, x)\} \in L(\mathbb{R})$ , we obtain by repeated integration by parts

$$q(x) = \left(\frac{i}{2\pi x}\right)^n \int dk \, \partial_k^{(n)}\{\rho(k)\varphi(k, x)\} e^{-2ikx}. \quad (4.10)$$

Hence finally

$$x \rightarrow \infty \quad \Rightarrow \quad x^n q(x) \rightarrow 0. \quad (4.11)$$

As mentioned in the introduction, such an asymptotic behavior is not found for the potential  $q_0(x, t)$  which would be obtained from TSRS with zero GVD (2.3). Indeed, in that case the medium initially at rest evolves universally towards the self-similar solution [11] which behaves as  $x^{-3/4}$  as found in [12]. More precisely we have

$$q \sim s(t) \xi^{-3/4} \left[ \alpha \cos(h\xi^{1/2} + \beta) + \mathcal{O}(\xi^{-1/2}) \right], \quad \xi = s(t) x, \quad (4.12)$$

where  $s(t)$  is a function of  $t$  determined by the boundary conditions and where  $\alpha, \beta$  and  $h$  are arbitrary constants.

Figure 4 presents the decay of  $|q|$  and  $|q_0|$  respectively in dashed line and full line as a function of  $x$  for  $t = T/2 = 50$  in a linear-log plot and the parameters (3.13). The exponential decay of  $|q|$  can be seen for all values of  $t$  and follows approximately  $e^{-\kappa x}$  as expected from the analysis. This observation justifies the fact that the finite length evolution of (2.2) is very close to the asymptotic expression (3.5) given by IST.

On the contrary the slow decay of  $|q_0|$  as  $x^{-3/4}$  makes it impossible for the integrals of (3.1) to exist so that the scattering theory must be revisited in this case.

## 4.4 Numerical spectral transform and Raman solitons

By numerical integration of the SRS system (2.2) with a spatial grid of dimension  $h$ , we get, at each value of time, a set of  $L$  discrete data  $q(n, t)$  (with  $x = nh$  and  $\ell = Lh$ ), that we now analyze by means of the spectral transform. This is easily done, using the results of [16] which, adapted to our notations, read

$$\rho(k, t) = R_0(\zeta, t) , \quad (4.13)$$

where  $R_0$  is obtained from the following inverse recursion

$$R_L = \zeta^L h q(L, t) , \quad R_{m-1} = \frac{R_m - h q(m-1, t) \zeta^{m-1}}{1 + R_m h \bar{q}(m-1, t) \zeta^{-m+1}} , \quad (4.14)$$

and where the parameter  $\zeta$  is related to  $k$  by

$$\zeta = e^{2ikh} . \quad (4.15)$$

It is then a simple task to use this recursion relation to compute the numerical spectral transform  $R_0(\zeta, t)$  and compare it to the asymptotic theoretical expression (3.10) of  $\rho(k, t)$ . In Figure 5 we plot  $|\rho(k, t)|$  where one can clearly see the three singularities  $(\zeta_n, t_n)$  for  $n = 0, 1, 2$  corresponding to the three poles of  $\rho$ .

The non linear spectral transform is easier to compute, faster and yields more information than the standard Fourier transform which in particular does not present any singularity (as we checked numerically).

## 5 Conclusion

This work demonstrates that the IST solution of transient SRS on the semi-infinite line furnishes a very accurate model for the solution on a finite domain. The accuracy stands not only for the output laser pulses intensities but also for their phases as shown in a spectacular way by the generation of the Raman solitons. It is shown that the question of the experimental observation of Raman solitons is solved by a convenient combination of the output (and input) laser profiles. We also performed a numerical *nonlinear spectral analysis* which resulted to be not only rich of information but also quite easy to implement and faster than the usual FFT procedure.

Finally we mention that it is difficult to compare these results with those obtained in the zero GVD case (2.3). The problem is that in the limit  $\kappa \rightarrow 0$ , the spectral transform gets an essential singularity in  $k = -i0$  which sends poles to the upper half-plane. To discuss the number and time location of such poles would require not only a careful study of the singular limit  $\kappa \rightarrow 0$ , but also to reformulate IST on the half-line as we have seen that the potential  $q(x)$  does not decrease *fast enough* as  $x \rightarrow \infty$ .

## Acknowledgments

JGC is on leave from the Laboratoire de Mathématiques de l'INSA de Rouen. The authors thank the CRIHAN computing center for the use of their facilities. We thank INTAS for support through grant 96-339 and support from Sezione INFN di Lecce and PRIN 97 "Sintesi".

## References

- [1] A.C. Newell, J.V. Moloney, *Nonlinear Optics*, Addison-Wesley (Redwood City CA, 1992)
- [2] A. Yariv, *Quantum Electronics*, J. Wiley (New York 1975)
- [3] F.Y.F. Chu, A.C. Scott, Phys. Rev. A **12** (1975) 2060
- [4] G.P. Agrawal, *Nonlinear optics*, Academic Press (London 1989)
- [5] K. Drühl, R.G. Wenzel, J.L. Carlsten, Phys. Rev. Lett., **51** (1983) 1171; R.G. Wenzel, J.L. Carlsten, K. Drühl, J. Stat. Phys., **39** (1985) 621
- [6] C. Claude, J. Leon, Phys. Rev. Lett., **74** (1995) 3479; C. Claude, F. Ginovart, J. Leon, Phys. Rev. A **52** (1995) 767
- [7] D.J. Kaup, Physica **6D** (1983) 143
- [8] H. Steudel, Quantum Opt., **2** (1990) 387
- [9] J. Leon, Phys. Lett. A **170** (1992) 283; Phys. Rev. A **47** (1993) 3264; J. Math. Phys., **35** (1994) 3054
- [10] D.E. Gakhovich, A.S. Grabchikov, V.A. Orlovich, Optics Comm., **102** (1993) 485
- [11] A.S. Fokas and C.R. Menyuk, J. nonlinear Sci., **9** (1999) 1
- [12] C.R. Menyuk, D. Levi, P. Winternitz, Phys. Rev. Lett. **69** (1992) 3048; D. Levi, C.R. Menyuk, P. Winternitz, Phys. Rev. A **44** (1991) 6057
- [13] C.R. Menyuk, Phys. Rev. A, **47** (1993) 2235
- [14] *Self-similarity in stimulated Raman scattering*, eds. D. Levi, C.R. Menyuk, P. Winternitz, Les Publications CRM (Montreal 1994)
- [15] J. Leon, A.V. Mikhailov, Phys. Lett. A. **253** (1999) 33
- [16] M. Boiti, J. Leon, F. Pempinelli, Phys. Rev. E **54** (1996) 5739. M. Boiti, F. Pempinelli, Inverse Problems **13** (1997) 919

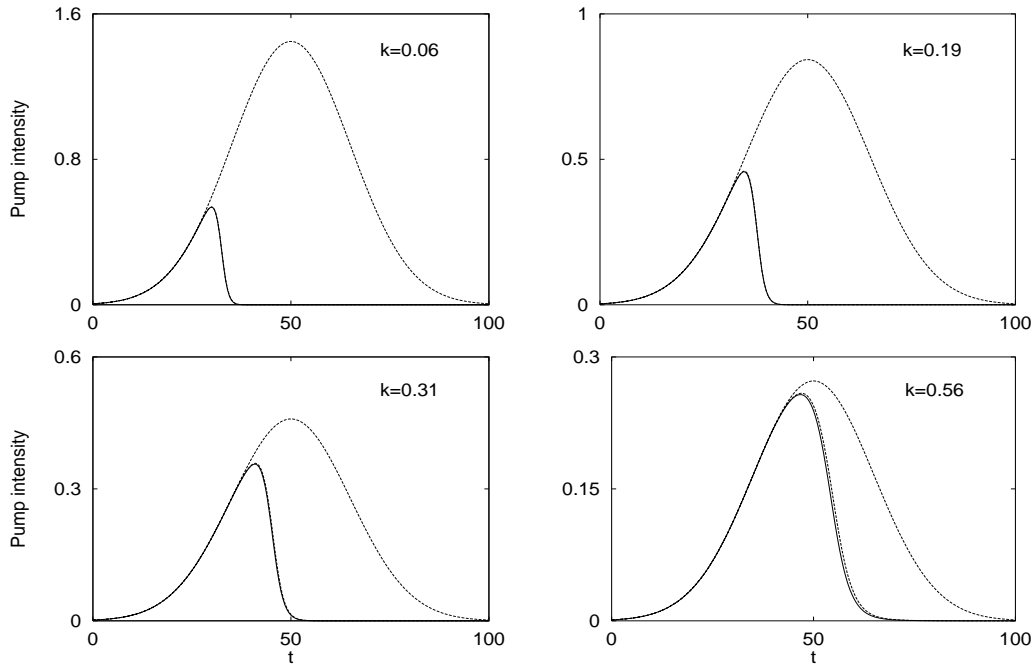


Figure 1: Plot, as functions of time, of the output pump intensity  $|a(x = \ell, k, t)|^2$  from the theoretical expression (3.5) (full line) and the numerical solution of (2.2) (dashed line) for four different values of  $k$ . The large gaussian curves (dashed line) represent the input pump intensities  $|a(x = 0, k, t)|^2$ .

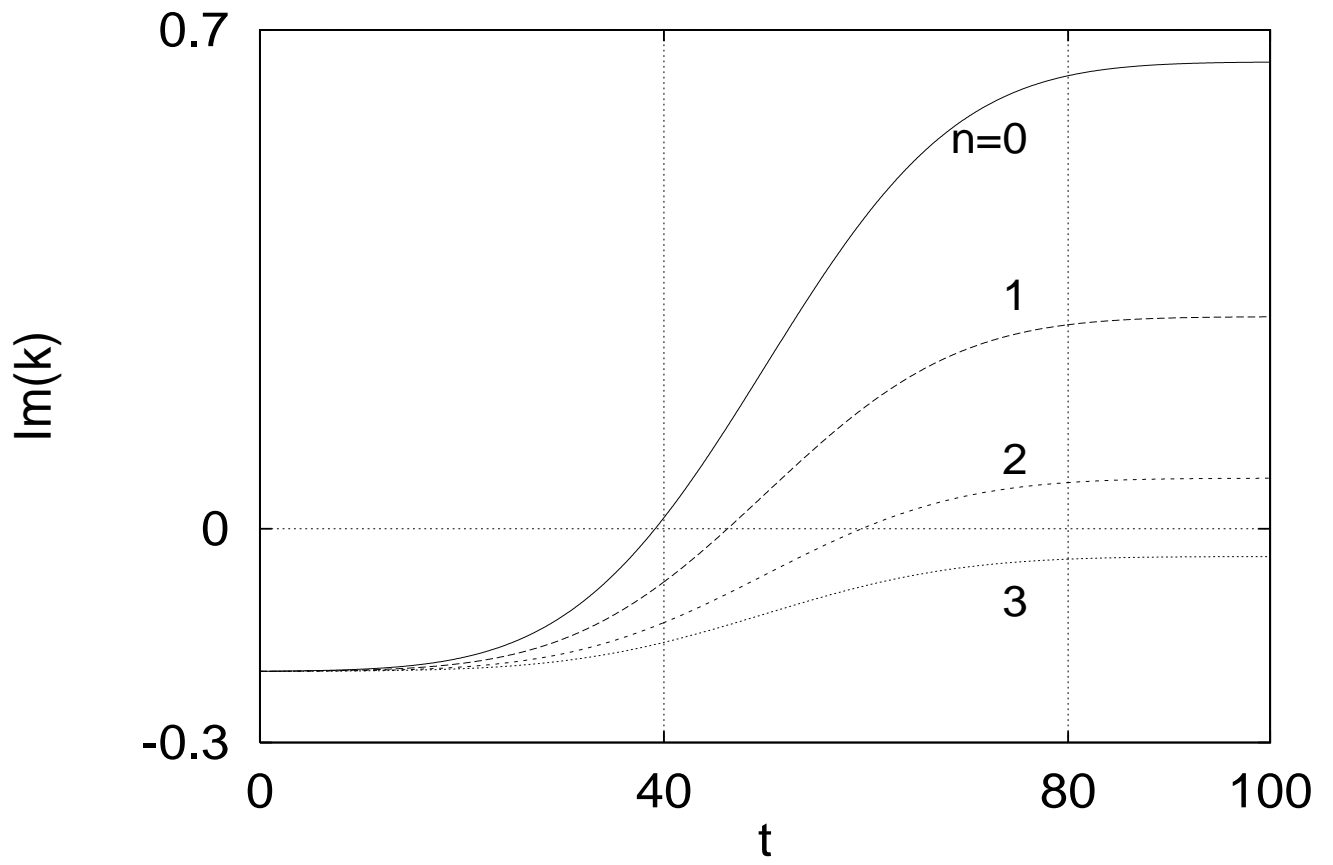


Figure 2: Time evolution of the imaginary part of the poles  $k_n$  of  $\rho$  for  $n = 0, 1, 2$  and 3. The parameters are the same as in Figure 1

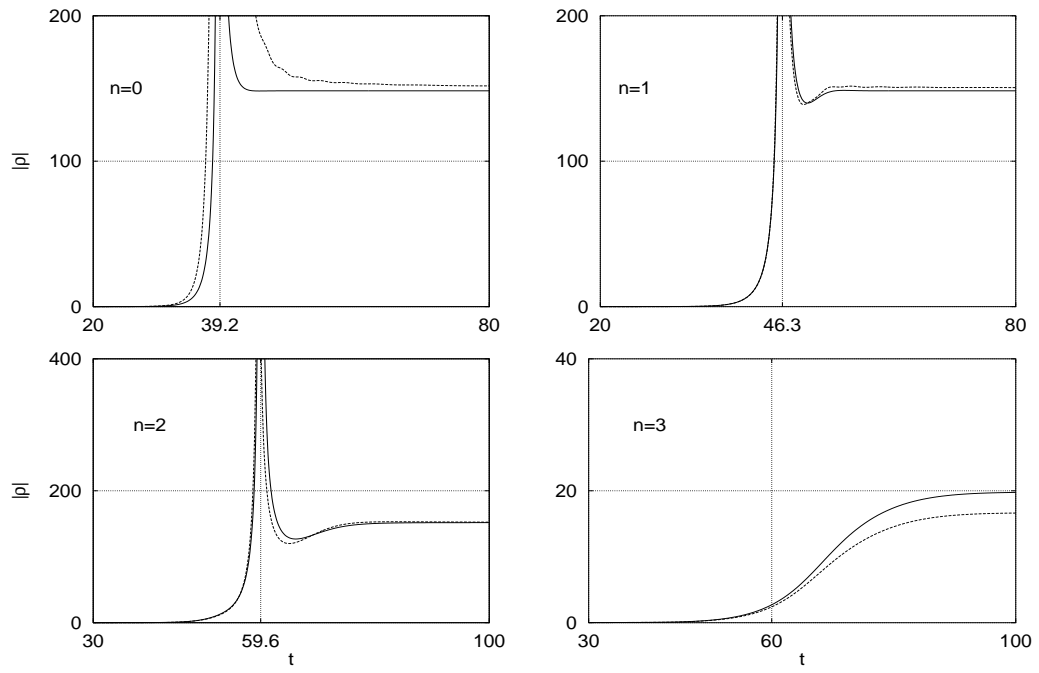


Figure 3: Time evolution of the reflection coefficient  $|\rho(\zeta_n)|$  for  $n = 0, 1, 2$  and  $3$  obtained from the inverse scattering theory (3.10) (full line) and from the numerical solution of (2.2) using formula (3.20) (dashed line).



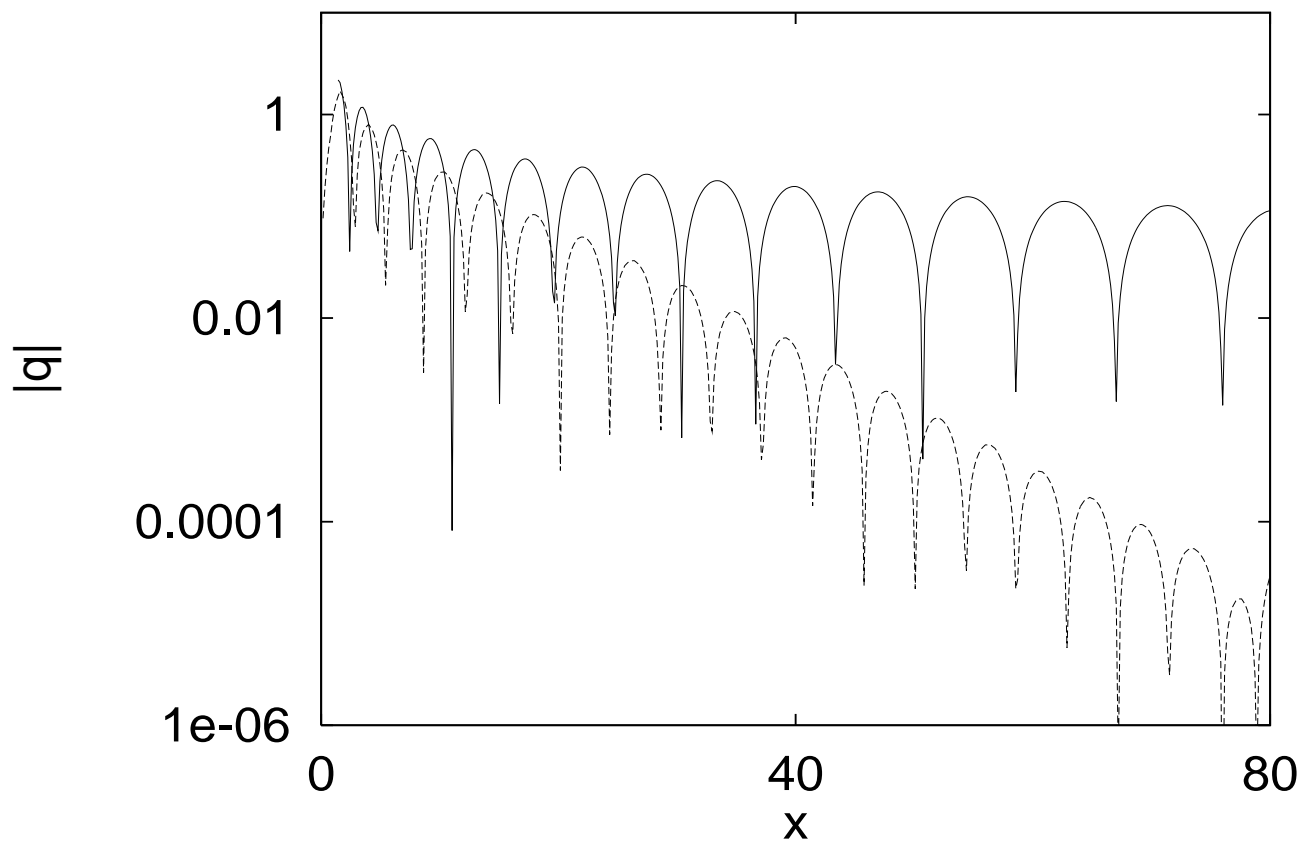


Figure 4: Evolution of  $|q|(x, t = 50)$  and  $|q_0|(x, t = 50)$  in linear-log coordinates.

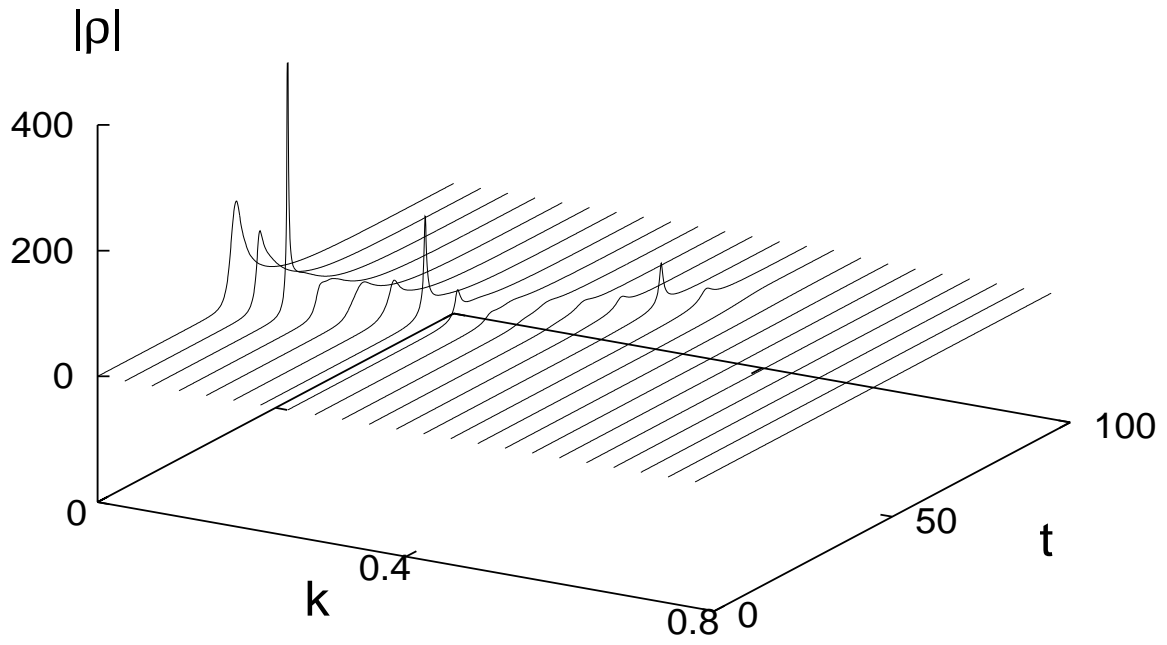


Figure 5: Evolution of  $|\rho|(k, t)$  obtained from the discrete spectral transform (4.13).